Formation of Pancreatic Islets Involves Coordinated Expansion of Small Islets and Fission of Large Interconnected Islet-like Structures

Junghyo Jo,[†*] German Kilimnik,[‡] Abraham Kim,[‡] Charles Guo,[‡] Vipul Periwal,[†*] and Manami Hara[‡*]
[†]Laboratory of Biological Modeling, National Institute of Diabetes and Digestive and Kidney Diseases, National Institutes of Health, Bethesda, Maryland; and [‡]Department of Medicine, The University of Chicago, Chicago, Illinois

ABSTRACT The islets of Langerhans, micro-organs for maintaining glucose homeostasis, range in size from small clusters of <10 cells to large islets consisting of several thousand endocrine cells. Islet size distributions among various species are similar and independent of body size, suggesting an intrinsic limit to islet size. Little is known about the mechanisms regulating islet size. We have carried out a comprehensive analysis of changes of islet size distribution in the intact mouse pancreas from birth to eight months, including mathematical modeling to quantify this dynamic biological process. Islet growth was size-dependent during development, with preferential expansion of smaller islets and fission of large interconnected islet-like structures occurring most actively at approximately three weeks of age at the time of weaning. The process of islet formation was complete by four weeks with little or no new islet formation thereafter, and all the β-cells had low proliferation potential in the adult, regardless of islet size. Similarly, in insulinoma-bearing mice, the early postnatal developmental process including fission followed the same time course with no new islet formation in adults. However, tumor progression led to uncontrolled islet growth with accelerated expansion of larger islets. Thus, islet formation and growth is a tightly regulated process involving preferential expansion of small islets and fission of large interconnected islet-like structures.

INTRODUCTION

Pancreatic islets are highly vascularized endocrine micro-organs composed of several hormone-secreting endocrine cells such as α (glucagon), β (insulin), and δ (somatostatin), PP (pancreatic polypeptide), and ε (ghrelin) cells that are embedded in the exocrine tissue and comprise 1–2% of the entire pancreas volume. Islet size varies from small cell clusters to large islets. In large animals, including humans, a proportionate increase in the pancreas size, islet number, and total islet mass compensates for an increased demand for insulin (1,2). However, as we have recently shown, there is no increase in the range of islet sizes in humans compared to those in mice and various other species (3,4). Indeed, upper and lower critical sizes for islet function have been reported: smaller islets (<1000 cells) can secrete more insulin per unit islet volume and have higher viability for islet transplantation in rats (5) and in humans (6), while some minimal clustering of cells is necessary for efficient insulin secretion (7–9). Collectively, these observations suggest that there are regulatory mechanisms that maintain optimal islet sizes in order to ensure their functional properties.

We reasoned that the developmental process of islet formation and subsequent islet growth holds key clues to understanding the mechanisms regulating functional islet size. To capture this dynamic process, we carried out a computer-assisted large-scale analysis of the entire distribution of islets in the intact mouse pancreas (10–12) and used this precise data for mathematical modeling of islet development. Our method identifies every islet within the intact pancreas with a specific identification number and provides multiple parameters such as islet area, circularity, and center coordinates: Circularity characterizes the shape of each islet, and center coordinates depict the spatial location of each islet in the whole pancreas. We utilized these parameters in the mathematical analysis of the fission of elongated interconnected islet-like structures and the subsequent spherical growth of islets during maturation. Here we develop an explicit mathematical model of the dynamic process of islet development based on the quantitative deduction of the recruitment rate of new islets and the size-dependent islet growth and fission rates. Acting in concert, these processes provide a tight regulatory mechanism for the islet size distribution.

MATERIALS AND METHODS

Mice

Mouse pancreata were excised from male/female (CD-1 background) transgenic mice in which pancreatic β-cells were endogenously tagged with green fluorescent protein (GFP) under the control of mouse insulin I promoter (MIP) (13,14). For generating insulinoma mice, MIP-GFP mice were further crossed with rat insulin II promoter (RIP)-Tag mice (15). The MIP-GFP and insulinoma mice are depicted as wild-type (WT) and RIP-Tag mice, respectively. All the procedures involving mice were approved by The University of Chicago Institutional Animal Care and Use Committee.

Preparation of specimens

Pancreata were removed intact with surrounding tissues such as spleen and duodenum, placed onto a standard glass slide flat to retain the orientation

Submitted May 16, 2011, and accepted for publication June 27, 2011.

*Correspondence: jojunghyo@mail.nih.gov or vipulp@niddk.nih.gov or mhara@midway.uchicago.edu

Editor: Richard Bertram.

0006-3495/11/08/0565/10 $2.00

doi: 10.1016/j.bpj.2011.06.042

(i.e., dorsal and ventral pancreas), then surrounding tissues were carefully removed. Pancreata were fixed with 4% paraformaldehyde at 4°C for overnight and permeabilized with 1% Triton-X 100 for two days. Specimens were further treated with saturated sucrose for several days, followed by 100% glycerol in order to clear tissue and obtain better resolution of fluorescent signals.

Imaging and quantification of β-cell area in the intact pancreas

Optical images of pancreata were obtained using an Olympus IX-80 (Olympus, Melville, NY) and software StereoInvestigator (MicroBrightField, Williston, VT). A ×2 objective lens was used to capture the entire adult (>3 months old) pancreas (~3 × 5 cm) on a glass slide, which allows us to scan through ~1 mm thickness of a specimen. For a smaller specimen size, a ×10 objective was used with a pair of 35-mm cover glasses. Three 3-month-old specimens were observed under both ×2 and ×10 objective lens to check resolution dependence. Detailed methods of image capturing and analysis are previously described (10–12).

Briefly, using a Virtual Slice module of StereoInvestigator (MicroBrightField), a contour is first manually drawn to encircle a whole pancreas, then the software starts to capture each optical panel sequentially by controlling a motorized stage in the XY axes until it covers an area of the drawn contour. In each capture of a panel, a focal plane (i.e., the Z axis) is selected manually to capture the best plane (i.e., the most populated area in a given depth of a specimen). Then StereoInvestigator creates a montage combining all the panels, which is designated as a "Virtual Slice". A resulting Virtual Slice is an integrated two-dimensional image like a bird's-eye view, although it is not a maximum projection from the three-dimensional reconstruction of the whole pancreas. Note that images are captured using the epifluorescent configuration (i.e., wide-field filters), but not the confocal mode, which limits a capture to a single focal plane. The epifluorescent configuration allows us to capture signals in certain depth, including those that are not in perfect focus. Image analysis was carried out using ImageJ (National Institutes of Health (NIH), Bethesda, MD).

Cell replication

Pancreas tissues were prepared from P3 ($N = 20$), P14 ($N = 9$), and P21 ($N = 7$). These specimens were paraffin-embedded and sections were cut in 5 μm in thickness. The sections were stained with a polyclonal guinea pig anti-porcine insulin primary antibody (DAKO, Carpinteria, CA), a polyclonal rabbit anti-phospho-histone H3 primary antibody (Chemicon, Temecula, CA), and DAPI (Invitrogen, Carlsbad, CA). The primary antibodies were detected using a combination of DyLight 488- and 549-conjugated secondary antibodies (Jackson ImmunoResearch Laboratories, West Grove, PA). Microscopic images were taken with an IX8 DSU spinning disk confocal microscope (Olympus, Melville, NY). Image analysis was carried out using ImageJ (National Institutes of Health).

Mathematical model

We introduce a mathematical model to examine birth, growth, and fission of islets that result in changes in islet size distribution as schematically described in Fig. 1. The number of islets, n_i, at a certain size, S_i, increases due to the growth of smaller islets of size S_{i-1} and the fission of larger islets of size S_j ($>S_i$). Here the number change is proportional to both the growth/fission rate and current islet number at the specific sizes. In addition, when the size is at its minimum, S_0, then the recruitment of new islets, defined as birth, contributes to increase the islet number at the size S_0. On the other hand, the growth or fission of islets of size S_i decreases the islet number at the same size S_i. These processes are summarized in the following discrete equation:

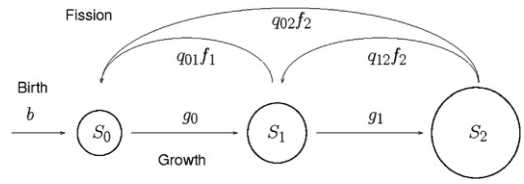

FIGURE 1 Schematic diagram of the mathematical model for islet development. The model describes islet development in terms of birth, growth, and fission. New islets appear with a birth rate, b, at the minimal islet size, S_0. Then, islets grow and fission with rates g_i and f_i, respectively, depending on islet size S_i. For the islet fission, the splitting matrix q_{ij} determines the probability that an islet with size S_j fission into an islet with size S_i.

$$n_i(t+\delta t) = n_i(t) + b\delta_{i,0} + g_{i-1}n_{i-1}(t) - g_i n_i(t) + \sum_{j>i} q_{ij} f_j n_j(t) - f_i n_i(t). \quad (1)$$

First, the recruitment of new islets at the minimal size S_0 is described by the Krönecker delta function: $\delta_{\iota,0}$ is 1 only if $i = 0$, and is otherwise 0. Here a birth rate parameter, b, is introduced to quantify how many new islets are recruited in a time interval, $\delta t = 1$ day. Second, the model considers size-dependent growth rate of islets with a simple exponential form, $g_i = \overline{g}e^{-S_i/\lambda_g}$, which is flexible enough to describe an increasing/decreasing growth rate with islet size, depending on the sign of the characteristic size scale, λ_g. Note that a large value of λ_g can also practically describe size-independent growth rate. Whereas the parameter λ_g parameterizes the size dependence of islet growth, the parameter $\overline{g}$ controls the magnitude of islet growth. Finally, we include the possibility of islet fission. The assumption that larger islets are more susceptible to fission is incorporated via a sigmoidal function of islet size, $f_i = \overline{f}/2[1 + \tanh((S_i - S_f)/\eta_f)]$, where $\overline{f}$ is the maximal fission rate; S_f is the critical size that gives a half-maximal fission rate; and η_f is the steepness of the size dependence.

For the occurrence of islet fission with a given fission rate, we consider the two simplest possible ways that an islet may split: symmetric fission and random fission. For symmetric fission, an islet of area A divides into two islets of area $A/2$. This is a reasonable assumption, when we consider fission from an elongated islet into two relatively spherical islets, rather than fission from a spherical islet into two spherical islets. In this study, we use a logarithmic size, $\log_2\tilde{A}$, of dimensionless islet area, $\tilde{A}$= islet area/single-cell area. In the analysis, we consider islets of which size is larger than a cutoff area, $\log_2\tilde{A}>2$. Then, each size bin S_i corresponds to islets of area, $(i+2)<\log_2\tilde{A}\le(i+3)$. In the logarithmic size scale, an islet of size $S_i = \log_2\tilde{A}$ symmetrically divides into two islets of size $S_{i-1} = \log_2(\tilde{A}/2)$. For random fission, on the other hand, an islet divides into two islets of any size with the same probability. In the logarithmic size scale, however, the probability increases exponentially with size, because size intervals between bins increase exponentially. These features for islet fission are described with the splitting matrices q_{ij} in Eq. 1: $q_{ij} = 2\delta_{i,j-1}$ for symmetric fission; $q_{ij} = 2\cdot 2^i/(2^j-1)$ for random fission. Note that these splitting matrices have a constraint, $\sum_{i=0}^{j-1} q_{ij} = 2$, due to the assumption of binary fission. In this study, we generally use time-dependent birth, growth, and fission rates ($b(t)$, $\overline{g}(t)$, and $\overline{f}(t)$, respectively) to describe a rapid change in early neonatal development, while we use them as constant rates to describe a slow change in late neonatal development.

Mean islet size distribution

Absolute frequencies, n_i, of islet sizes at a given time showed a large variation between mice as the large variation in total islet number between mice. On the other hand, the relative frequencies, p_i^I, of islet size, S_i,

between different mice ($l = 1, 2, \ldots, N$) showed a small variation. Therefore, we obtained absolute frequencies using the homogeneous relative frequencies with a multiplication of the scale factor, the predicted total islet number: $n_{tot}(t) = 305 + 993(1 - \exp(-t/12.2))$ for WT mice; $n_{tot}(t) = 570 + 1113(1 - \exp(-t/26.5))$ for RIP-Tag mice where time t has a unit of day. Therefore, the mean absolute frequencies of islet size, n_i, and its uncertainty, δn_i, at a given time are calculated as follows: $n_i = n_{tot}\frac{1}{N}\sum_{l=1}^{N} p_i^l$ and $\delta n_i = n_{tot}\sqrt{\frac{1}{N}\sum_{l=1}^{N}(p_i^l - \overline{p}_i)^2}$ with $\overline{p}_i = \frac{1}{N}\sum_{l=1}^{N} p_i^l$.

Optimization of model parameters

The mathematical model describes changes of islet size distribution, $n_i(t)$, starting from an initial size distribution, $n_i(t_0)$. With a given parameter set, $\vec{x} = (b_k, \overline{g}_k, \lambda_g, \overline{f}_k, S_f, \eta_f)$, the model simulation predicts time evolutions of the distribution, $\widehat{n}_i(t_k)$, starting from an initial distribution, $n_i(t_{k-1})$. Here the index, $k = 1, \ldots, m$, indicates time dependence of m time steps. Note that as an initial distribution for each time interval, we used measured distributions, $n_i(t_{k-1})$ instead of predicted distributions $\widehat{n}_i(t_{k-1})$ so as not to accumulate simulation errors. Then, we compare these predicted distributions, $\widehat{n}_i(t)$, with measured distributions, $n_i(t)$, and quantify the entire discrepancy as a cost:

$$E = \sum_{k=1}^{m}\sum_{i=0}\frac{[n_i(t_k) - \widehat{n}_i(t_k)]^2}{\delta n_i^2(t_k)}. \quad (2)$$

Note that the cost, E, is scaled by the uncertainty, $\delta n_i(t)$, of the measured size distributions. For the parameter optimization to match the predicted and measured size distributions (or to minimize the cost), we used the parallel tempering Monte Carlo (MC) method (16). For the islet development of WT mice, starting from an initial islet size distribution at postnatal day 1 (P1), we optimize the parameters to match the measured distributions at P3, P5, P7, P10, P12, P14, P18, and P21 that correspond to $m = 8$ time steps; for RIP-Tag mice, we have an initial distribution at P3 and following distributions at P4, P5, P6, P7, P9, P10, P12, P14, P16, and P18 with time steps $m = 10$. Differently from this early postnatal period in which rapid developmental changes occur, after week 4 (P28), the islet growth is slow enough to neglect time dependence of the growth process; $b_k = b$, $\overline{g}_k = \overline{g}$, and $\overline{f}_k = \overline{f}$. For WT mice, we now start from postnatal week 3 (W3) and optimize the parameters to match the measured distributions at W4, W8, W12, W16, and W20 with $m = 5$, whereasfor RIP-Tag mice, starting from W3, we have the following distributions at W4, W5, W8, W10, W15, and W20 with $m = 6$. Note that for the simulation of late islet development, we used fixed total islet numbers, with $n_{tot} = 1268$ and 875 for WT and RIP-Tag mice, respectively (see Fig. S3 in the Supporting Material).

For the parallel tempering MC simulation, we set 10 uniformly spaced values (0.1–1) for the tempering parameter Θ_u and ran 10 chains ($u = 1, 2, \ldots, 10$) in parallel with updating probability $\exp[-\Theta_u E(\vec{x}_u)]$. At every 20 steps, we randomly picked two chains of different temperatures (Θ_u and Θ_v) and exchanged their parameter sets ($\vec{x}_u$ and $\vec{x}_v$) with a probability, $\exp[(\Theta_u - \Theta_v)(E(\vec{x}_u) - E(\vec{x}_v))]$, to find the global minimum of the cost more efficiently using the advantage of fine searching at low temperature and global searching at high temperature. After equilibration, we calculated likelihood values of parameters and cost by averaging the parameters and cost generated by 10^6 MC steps with a fixed temperature $\Theta = 1$. For the model comparison, we used the Bayesian model probability $P(M|D)$, which estimated how well a model describes given data (16). The probability can be calculated from the MC simulation with different temperatures: for 10 chains,

$$-\ln P(M|D) = \frac{1}{10}\sum_{u=1}^{10}\overline{E}_u, \quad (3)$$

where $\overline{E}_u$ represents the average cost for each temperature Θ_u. Note that for this calculation, there is no exchange between MC chains of different temperatures in contrast to the previous procedure for searching a global minimum of a cost function. We used 10^6 MC steps to determine the model probability.

RESULTS

Large-scale image analysis of pancreatic islets

The entire distribution of islets was captured in situ and analyzed (Fig. 2 *A*). The number and size of islets increased during the postnatal period. The islet distribution had

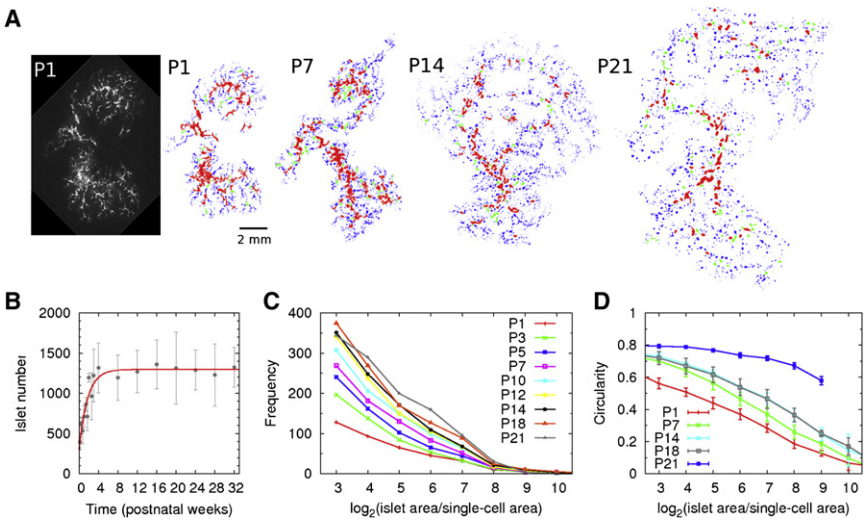

FIGURE 2 Large-scale image analysis of postnatal pancreatic islets. (*A*) A wide-field image of every fluorescent β-cell in an intact pancreas at postnatal day 1 (P1). Based on the confocal image, we identified cell clusters as islets using an image-analysis software, ImageJ (NIH), and colored each cluster depending on size: small (*blue*), intermediate (*green*), and large (*red*) islets. We used two different intensity thresholds to detect simultaneously both highly fluorescent large islets and dimmer small islets. The intermediate islets are detected with an average threshold value after the previously detected large and small islets are subtracted. These intermediate islets generally have sizes of ~30,000 μm^2. Representative islet distributions at P1, P7, P14, and P21 were plotted. (*B*) The total number of islets, defined as cell clusters (>4 cells), is fit with an increasing function, $n_{tot}(t) = 305 + 993(1 - \exp(-t/12.2))$ as time, t (day). (*C*) Histograms of islet size at P1–P21. Note that we measured absolute (not relative) frequencies of islet size in a pancreas. Islet size is represented as a logarithmic scale of islet area relative to single-cell area (170 μm^2). (*D*) Larger islets have more elongated shapes. Circularity is defined as $(4\pi A/P^2)$, with A being area and P being perimeter (which is the length of the outside boundary of a selected islet region) so that a circle has circularity 1. For these figures, 6–12 mice at each time point were used; mean ± SD.

a branching pattern with large interconnected islet structures accompanied with numerous small islets in the peripheral branches. Based on the measured area of cell clusters, we defined an islet as a cluster of >4 cells ($4 \times 170\ \mu m^2$) (14), because the detection of clusters larger than this cutoff size was consistent across magnification levels (see Fig. S1). Total islet number counts increased until postnatal week 4, after which they were constant (Fig. 2 *B*).

We also constructed histograms of islet sizes at various postnatal days (Fig. 2 *C*). The islet size distributions did not depend on gender of mice (data not shown). Note that these are absolute mean frequencies of islet sizes for a given pancreas (see Materials and Methods). In considering the analysis of the size distribution, we used a logarithmic size scale due to the high number of small islets and the low number of large islets. Islets of various sizes were distributed throughout the pancreas; the head, body, and tail regions maintained similar islet size distributions (see Fig. S2). Another interesting feature was the elongated structure of large islets compared to small islets (Fig. 2 *D*). In addition, islets become more circular with time. Accordingly, this observation led us to examine large islets in detail, whereupon we found that they have heterogeneous segmented areas delineated by the Watershed segmentation algorithm on the basis of fluorescent signal shape (Fig. 3 *A*). These large elongated multisegment islets have been also observed on neonatal pancreatic sections with immunohistochemistry (11). The number of segments decreased with time (Fig. 3 *B*). Both increasing circularity and decreasing segment number of large elongated islets suggest the occurrence of fission. Based on these observations of islet number, size, shape, and segments, it seems that new islets appear, grow, and then divide.

Mathematical modeling of neonatal islet development

We reasoned that these biological processes should lead to correlated changes in islet size distributions. Therefore, we developed a mathematical model to quantify the changes in terms of islet birth, growth, and fission. Specifically, we considered three potential models differing with respect to islet fission: 1), no fission, excluding occurrence of islet fission; 2), symmetric fission, assuming that an islet divides into two islets of similar size; and 3), random fission, assuming that an islet may divide into two islets of any size.

With a given data uncertainty, all three models could fit the changes in islet size distribution during the early postnatal period (Fig. 4 *A*). Based on the changes in islet size distribution, we quantitatively deduced growth and fission rates depending on islet size. Small islets grew faster than large islets in terms of islet area expansion. Islet growth rate was relatively large during early postnatal days but diminished with time. Large islets had a higher fission probability per unit time. In particular, the critical islet size, giving a half maximal fission rate, has an area including ~500 cells.

A dramatic increase in islet fission occurred around postnatal week 3 at the time of weaning. For the recruitment of new islets, defined as birth, on average 40 new islets appeared per day during initial postnatal days, but this diminished with time, and ceased after week 3 (Fig. 4 *B*), as indicated by the constant number of islets observed after that time point (Fig. 2 *B*). During the postnatal period, 800 new islets appeared (Fig. 2 *B*). Based on the islet birth rate, we estimated that 500 new islets resulted from islet birth and the remaining 300 new islets resulted from islet fission. Finally, using a Bayesian model comparison to determine which islet fission model is more likely to explain the given data, we concluded that the model of random islet fission is the most likely (Fig. 4 *C*). In particular, this model best explains the change in islet size distribution from postnatal day 18 to 21 when an enormous amount of islet fission occurred (Fig. 4 *A*).

Neonatal islet growth and fission

To confirm the model predictions of islet growth and fission, we checked them with independent measurements. For islet growth, we observed cell proliferation in islets of different sizes at postnatal day 3, 14, and 21. As estimated with the model, the cell proliferation rate decreased with time

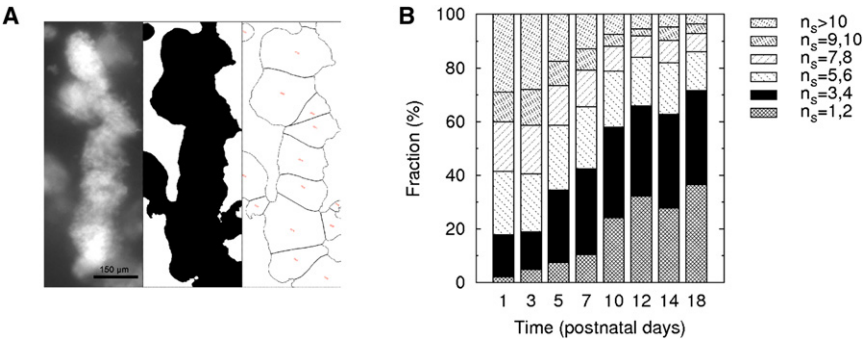

FIGURE 3 Segments in large islets. (*A*) An individual segment area of a large islet is outlined by Watershed segmentation algorithm. We counted segment number for each large islet. The scale bar is 150 μm. (*B*) Fraction of islets with different segment number, n_s, at P1–P18.

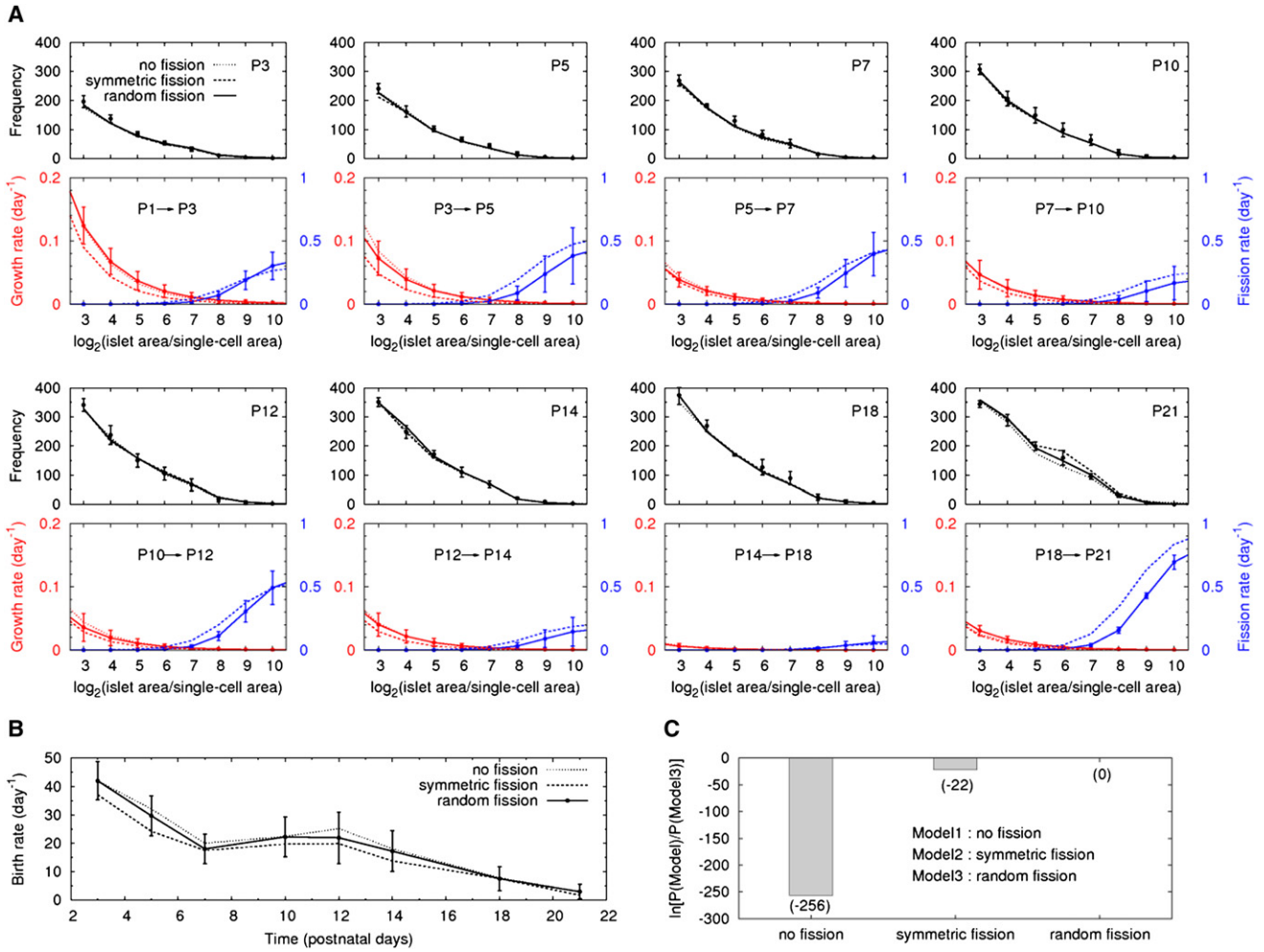

FIGURE 4 Birth, growth, and fission rates deduced from the mathematical modeling. (*A*) Absolute frequencies of islet size at P3–P21 are displayed (*circles* and *error bars*; mean ± SD; $N = 6$–12) with highest probability predictions of three models: Model 1, excluding islet fission process (*dotted line*); Model 2, considering symmetric islet fission (*dashed line*); and Model 3, considering random islet fission (*solid line*). Based on the changes of islet size distributions for a given period, likely growth (*red*) and fission (*blue*) rates depending on islet size are deduced. (*B*) Birth rates, quantifying how many new islets are recruited per day, are also deduced from the three models. Note that standard deviations are displayed only for the random fission model in order not to complicate the figure; the other models have similar degrees of standard deviation. (*C*) Bayesian model probabilities indicating which model is more likely to explain the given data. The model probability, $P(M|D)$, described in Materials and Methods, is abbreviated as $P(Model)$. Exact numbers of the logarithmic values of the relative model probability are shown in parentheses for clearer comparison.

(Fig. 5 *A*). In addition, cells replicated more frequently in smaller islets, but the size dependence was not statistically significant ($P > 0.05$). This suggests that the preferential expansion of smaller islets, which was observed particularly in early postnatal days (<P3) from changes of islet size distribution (Fig. 4 *A*), may not result from preferential cell proliferation in smaller islets, but from aggregation of small cell clusters during early development.

Next, to examine the occurrence of islet fission, we calculated distances between nearest-neighboring islets in pancreata at different postnatal days, using the center coordinates and size of each islet in a given pancreas. We hypothesized that if islet fission occurred, proximal pairs of the nearest-neighboring islets (recently divided islets) increased unless they quickly moved away from each other after division. Here the proximity of two islets was estimated by comparing the distance between them with the sum of their radii, by defining a threshold ratio $\varepsilon = d/(r_1 + r_2)$. Fig. 5 *B* showed proximal islet pairs in a pancreas at P21 under a threshold ratio $\varepsilon < 1.2$. Therefore, we quantified the fraction of the proximal islet pairs that were closer than a given threshold ratio (Fig. 5 *C*). A large threshold ratio detects every neighbor of every islet, while a small threshold ratio selects neighboring islets that have just been formed by fission and are still proximal.

When we used a large threshold ratio ($\varepsilon < 1.5$), the resultant subset of neighboring islets followed the general trend that neighboring islets moved away from each other during pancreas expansion and the fraction of proximal islet pairs decreased with time. On the other hand, when we used small

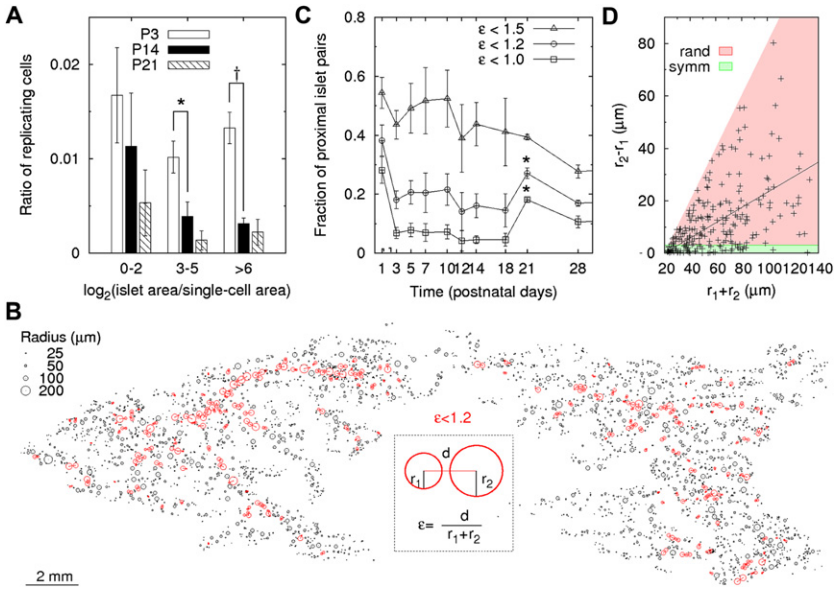

FIGURE 5 Experimental evidences for the model predictions of islet growth and fission. (*A*) Ratio of replicating cells in islets depending on islet size at P3 ($N = 20$), P14 ($N = 9$), and P21 ($N = 7$); mean ± SE. Here replicated cells are identified with the staining of anti-phospho-histone H3 primary antibody. $*P < 0.05$ and $\dagger P < 0.001$ (not 0.01). (*B*) Proximal islet pairs (*red circles*) are selected among nearest-neighboring islets. The proximity is estimated by the distance, d, between nearest-neighboring islets divided by the sum of their effective radii, $r_1 + r_2$. Here the effective radius is defined as a radius of a circular islet giving the same area of an original elongated islet. The ratio, $\varepsilon = d/(r_1 + r_2)$, quantifies how close the given nearest-neighboring islets are. For example, when two circles attach to each other, the ratio is $\varepsilon = 1$. Plotted is a representative example of a pancreas at P21 with a proximity threshold ratio ($\varepsilon < 1.2$). (*C*) Fraction of proximal islet pairs at different days during the postnatal period under three proximity threshold ratios, $\varepsilon < 1$, 1.2, and 1.5 are calculated. $*P < 0.001$ for P18 vs. P21. (*D*) Radius difference $r_2 - r_1$ of two proximal islet pairs ($r_2 > r_1$) in a pancreas at P21 under $\varepsilon < 1.2$. (*Black solid line*) Linear correlation between the difference and sum of the radii. Two idealized results of random (rand; *red region*) and symmetric (symm; *green region*) fissions are displayed as a reference.

threshold ratios ($\varepsilon < 1.0$ or 1.2), we could selectively detect the proximal islet pairs that had presumably just appeared as a result of fission. Indeed, we observed a markedly increased fraction of proximal islet pairs between postnatal day 18 and 21, as predicted from changes in islet size distribution (Fig. 4 *A*). Finally, we compared sizes (radii) of neighboring islet pairs under the threshold ratio $\varepsilon < 1.2$ (Fig. 5 *D*). The sizes of proximal islet pairs at postnatal day 21 were not symmetric, supporting random islet fission. If islets divide symmetrically, the radius difference between two proximal islets should be negligible. On the other hand, if islets divide randomly, the radius difference, $r_2 - r_1$, ($r_2 > r_1$), can be any value up to (approximately) $r_1 + r_2$. We observed a linear correlation between the radius difference and the sum of their radii (coefficient of determination $R^2 = 0.23$; $P < 0.0001$), supporting random islet fission rather than symmetric islet fission.

Limited islet growth in late development and adulthood

Islet development is limited after the early period of postnatal day 21. As a positive control, we examined the islet development of adult wild-type (WT) mice, and compared it with extreme islet outgrowth in insulinoma-bearing mice expressing oncogenic SV40 large T antigen (RIP-Tag) under the control of rat insulin II promoter (RIP) (15). In the early postnatal period, the insulinoma-bearing mice developed similarly to WT mice in terms of body weight, pancreas weight, islet number (see Fig. S3), and total β-cell area (Fig. 6 *A*). In addition, similar changes of islet size distribution occurred in RIP-Tag and WT mice (see Fig. S4). However, after eight weeks of age, the RIP-Tag mice started to show an outgrowth of islets. Based on changes in islet size distributions from weeks 3 to 20 (Fig. 6 *B*), we deduced the (assumed) constant islet growth rates of WT and RIP-Tag mice during the period (Fig. 6 *C*). The islets in RIP-Tag mice showed a larger growth rate compared to the limited islet growth in WT mice during this period. In particular, the size dependence of growth between them differs entirely: whereas small islets grow faster in WT mice, large islets grow faster in RIP-Tag mice. The preferential growth of larger islets in the tumor condition might result from a higher chance for spreading tumor cells in the larger cell populations or from a more extensive invagination of blood vessels to supply nutrients in the larger islets.

Note that islet birth and fission rates were negligible in both WT and RIP-Tag mice during this period, which is consistent with a previous report (17). Finally, we observed islet size distribution in 24–32-week-old adult mice (Fig. 7 *A*). The islet size distribution did not change during this late period (weeks 24–32), suggesting limited islet growth in adulthood. It is of particular interest that the islet size distribution fit a normal (or Gaussian) distribution. When the islet size distribution is plotted against islet diameter instead of the logarithmic scale of islet area, it fitted a log-normal distribution remarkably well (Fig. 7 *B*), compared with other skew distributions such as inverse Gaussian (or Wald), Weibull, and γ-distributions (Fig. 7 *C* and Table 1).

DISCUSSION

In this study, we developed a mathematical model to elucidate the intrinsic mechanisms for regulating islet size during

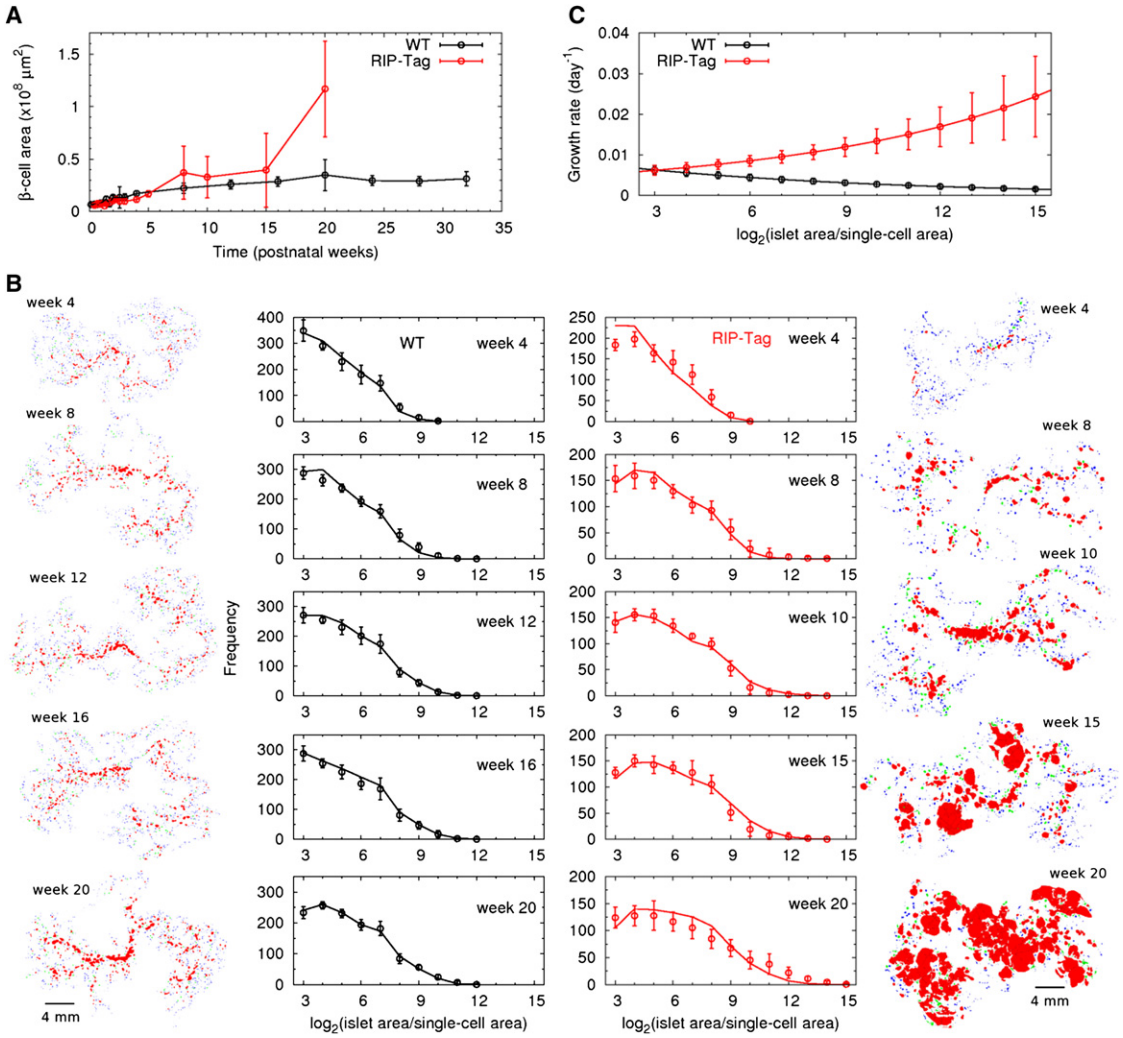

FIGURE 6 Islet growth in late development of wild-type and insulinoma mice. (*A*) Total β-cell area in a pancreas of wild-type (WT; *black*) and insulinoma (RIP-Tag; *red*) mice. Note that the RIP-Tag mice do not survive after postnatal week 20. (*B*) Measured absolute frequencies of islet sizes (*circles*) are compared with predicted frequencies from the mathematical model with random islet fission (*solid lines*) from week 4 to week 20 in WT (*black*) and RIP-Tag (*red*) mice. Representative pancreata with color-mapped islets are displayed parallel to corresponding islet size distributions: small (*blue*), intermediate (*green*), and large (*red*) islets. The result of RIP-Tag week 5 is omitted to match WT results in which week 5 was absent. The scale bars are 4 mm. (*C*) Size-dependent growth rate of islets in WT and RIP-Tag mice are deduced from changes of islet size distributions. For these figures, 6–12 mice at each time point were used; mean ± SD.

development. Our model delineates the complex process of islet formation that involves time-dependent islet birth, both time- and size-dependent islet growth, and fission. Diminishing islet birth, preferential growth of small islets, and fission of large interconnected islet-like structures during the postnatal period result in a tight range of islet sizes that best fits a log-normal distribution. The mathematical model is simple, but elaborate enough to extract important parameters that have never been extracted from direct experiments: islet growth and fission rates; their size dependences; and relative contribution of islet birth and fission to the increase of islet number during the postnatal period. Although more mathematically sophisticated models are trivially devised, we have restricted ourselves to the simple model presented here to avoid overfitting the data available at present. Our simple model can be a minimal basis for further study, although we obviously cannot completely rule out alternative explanations of changes of islet size distribution with more complex mechanisms, e.g., simultaneous occurrence of islet fusion and fission with complicated size- and time-dependence.

Large-scale analysis of the entire distribution of islets in the intact mouse pancreas has provided multiple parameters to precisely quantify the rates of new islet formation, growth, and fission events with spatial information of each islet in the whole pancreas. Such detailed information is not readily obtained using the conventional method of estimating the islet size distribution with selected histological tissue sections or isolated islets (18,19). Recently, optical projection tomography of pancreatic islets has also provided

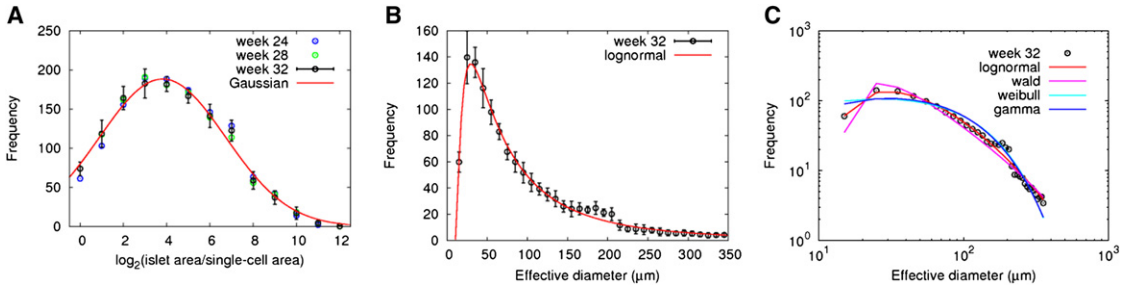

FIGURE 7 Islet size distributions in adult mice. (*A*) Islet size distributions at 24, 28, and 32 weeks old ($N = 6$–12; mean ± SD). For simplicity, its standard deviation is plotted only at 32 weeks because those of the other ages are similar. The size distribution at 32 weeks old was fitted with a Gaussian function (*red line*). (*B*) Islet size distribution of 32-week-old mice is fitted with a log-normal distribution. Here islet size is represented as effective diameter giving the same area as measured islet area. (*C*) Comparison of different fitting functions for islet size distributions: log-normal, inverse-Gaussian (Wald), Weibull, and γ-distributions. Details of each functional form and most-likelihood parameter values are summarized in Table 1. Log-log plots are used for a clearer comparison.

precise measurements of islet sizes in an intact pancreas (20). Our method used two-dimensional epifluorescent images in single focal planes across the intact pancreas under a coverslip to capture every islet. Although this two-dimensional observation might not detect some islets masked by other islets on top of them, most islets (especially large islets) are taken into account under the coverslip because we have checked that our method and the optical projection tomography method (21) are in good agreement with respect to islet size distributions as well as total islet number in three-week-old mice despite the strain difference between CD-1 and nondiabetic NOD.B10-H-2b backgrounds, respectively. Another possible concern is that the coverslip might flatten islets. As visible islet area does not change much until a space of 0.3-mm depth between a glass slide and the coverslip is reached (22), this flattening does not affect the vast majority (95%) of islets that have diameters <0.3 mm.

Little is known about the mechanisms of islet formation and the regulation of islet number and size distribution. The determinants of islet formation during development and the appearance of new islets in the adult are currently controversial issues in the field of β-cell biology. These processes have important implications for the development of therapeutic interventions for the treatment of diabetes, including islet regeneration and stem/progenitor cell therapies. The widely accepted model of islet formation is the local aggregation of endocrine cells, which migrate from the ductal epithelium in the late embryonic stage (reviewed in Kim and Hebrok (23)). This model conceptually supports possible new islet formation in the adult from injury-induced endocrine progenitor cells in the ductal epithelium (24–27). However, we have shown that total islet number does not change after four weeks of age in wild-type as well as insulinoma-bearing mice, suggesting that islet formation is complete at this point. The finding does not exclude the possibility of islet neogenesis under extreme experimental conditions such as chemically or surgically induced damage of the pancreas. However, this possibility has not been demonstrated under physiological conditions, and a number of studies contradict it (28–30).

Scaglia et al. (31) reported no β-cell mass increase in neonatal rats until P20, which was described as being due to concomitant replication and apoptosis. However, we did not observe such a plateau in β-cell mass in mice, which consistently increased during development. Our results are

TABLE 1 Normalized fitting functions for islet size distribution in adulthood

		Max-likelihood parameter value		
	Functional form	a	b	Log (model probability)
Log-normal	$\frac{1}{sb\sqrt{2\pi}}\exp\left[-\frac{\ln s - a}{2b^2}\right]$	4.1	1.1	0
Inverse Gaussian (Wald)	$\left(\frac{b}{2\pi s^3}\right)^{1/2}\exp\left[-\frac{-b(s-a)^2}{2a^2 s}\right]$	117.5	49.5	−36.2
Gamma	$\frac{s^{b-1}}{a^b\Gamma(b)}\exp\left[-\frac{s}{a}\right]$	68.2	1.3	−47.3
Weibull	$\frac{b}{a}\left(\frac{s}{a}\right)^{b-1}\exp\left[-\left(\frac{s}{a}\right)^b\right]$	92.9	1.1	−61.0

Here the size variable, s ($= d - d_0$), stands for islet diameter, d, subtracting a cutoff size, $d_0 = 10$ μm, below which no single cells can be found. Model probability, $P(M|D)$, explaining which model is more likely to explain a given data, was obtained by a Bayesian model comparison. Every model probability was represented as a relative value to the most-likelihood model, Log-normal function.

based on observed changes in islet size, the net result of all processes that affect β-cell mass. Whereas islet growth was relatively large during early postnatal days (<4 weeks), it diminished with time and became very slow after the early period, in accord with reports that β-cells turn over very slowly in aged mice (32). Chitinne et al. (33) has recently emphasized the contribution (>90%) of postnatal islet formation and growth in the total β-cell mass in adult rats. Consistent with this observation, our study showed that 80% of total β-cell mass in adult mice resulted from postnatal islet formation and growth. Because of the slow replication of β-cells in adults, identification of stem/progenitor cells is an important issue for restoring β-cell mass in diabetes. Brennand et al. (34) have reported that every β-cell contributes equally to islet growth and maintenance. However, our analysis of islet size distributions showed that small islets grew faster than large islets, albeit with minor size dependence in late development. Nevertheless, cell replication measurements failed to show preferential cell replication in smaller islets within a large variation between islets.

In embryonic development, aggregation of cell clusters, i.e., fusion, may occur considering the polyclonal origin of islet cells (35,36). Branched cordlike islet structures in embryo may result from such aggregation. At postnatal day 1, the largest islet has 1000-times larger area than small islets. It is implausible that this huge size difference is simply due to heterogeneous cell proliferation, suggesting the possibility of islet fusion during embryonic stages. Furthermore, the morphology of large islets, which seem to have interconnected segments, also supports the occurrence of islet fusion. This morphological feature of large islets may not be an artifact of the overlapping fluorescent islets observed on a focal plane, because it has also been observed on pancreatic sections with immunohistochemistry (11). However, islet fusion in the postnatal period is probably unimportant based on three observations: 1), the total number of islets increases and finally becomes constant in the adult; 2), islets become more circular with time; and 3), the number of segments in a given islet decreases.

These observations support the occurrence of islet fission rather than islet fusion during the postnatal period. Thus the fission of large interconnected islet-like structures can explain the drastic morphological difference between embryonic endocrine cell proliferation in the form of branched cordlike structures and the spherical-shaped islets observed in the adult (11).

Islet fission via "dumbbell islets" has been proposed by Seymour et al. (37) who described a cell composition analysis using pancreatic sections from H253 X-inactivation mosaic mice. They reported the transition of heterogeneous cell composition in the early neonatal period toward monoclonality in the adult and proposed islet fission as a mode of islet production, where frequently observed large "dumbbell-shaped" islets represented a state of fission in the postnatal pancreas. We speculate that the authors might have captured "interconnected islet-like structures" as dumbbell islets using a standard histological method, which technically limits observations within selected thinly cut tissue sections. In fact, interconnected islet-like structures are composed of many segments (i.e., more than two), and the fraction of the largest segment area varies. Furthermore, fission events are not symmetric but random, contravening a simple split of outgrown large islets into two. Therefore, islet fission may be a passive process in which interconnected islet-like structures just split into segments due to the relatively rapid expansion of the exocrine tissue rather than an active process in which a spherical islet divides into two spherical islets with an intermediate dumbbell-shaped stage. It has been reported that whereas the proliferation rate of endocrine cells rapidly decreases after birth, the proliferation of exocrine cells continues for a longer period to increase pancreas volume (11).

Our mathematical model demonstrates the dynamic process of neonatal islet formation and the coordinated regulation of islet number and size distribution. Mathematical modeling based on large-scale data provides a powerful tool to examine complex biological processes. Our work lays the foundation for future studies of various conditions such as pregnancy, obesity, diabetes, and aging.

SUPPORTING MATERIAL

Four figures are available at http://www.biophysj.org/biophysj/supplemental/S0006-3495(11)00772-7.

We thank Ulf Ahlgren for kindly providing data measuring islet sizes with optical projection tomography, and Arthur Sherman and James Johnson for a critical reading of the manuscript.

The study is supported by U.S. Public Health Service DK-081527, DK-072473, and DK-20595 to The University of Chicago Diabetes Research and Training Center (Animal Models Core), a gift from the Kovler Family Foundation, and funding from the intramural research program of the National Institutes of Health, National Institute of Diabetes and Digestive and Kidney Diseases.

REFERENCES

1. Bonner-Weir, S. 1994. Regulation of pancreatic β-cell mass in vivo. *Recent Prog. Horm. Res.* 49:91–104.
2. Montanya, E., V. Nacher, …, J. Soler. 2000. Linear correlation between β -cell mass and body weight throughout the lifespan in Lewis rats: role of β-cell hyperplasia and hypertrophy. *Diabetes.* 49:1341–1346.
3. Kim, A., K. Miller, …, M. Hara. 2009. Islet architecture: a comparative study. *Islets.* 1:129–136.
4. Steiner, D. J., A. Kim, …, M. Hara. 2010. Pancreatic islet plasticity: interspecies comparison of islet architecture and composition. *Islets.* 2:135–145.
5. MacGregor, R. R., S. J. Williams, …, L. Stehno-Bittel. 2006. Small rat islets are superior to large islets in in vitro function and in transplantation outcomes. *Am. J. Physiol. Endocrinol. Metab.* 290:E771–E779.
6. Lehmann, R., R. A. Zuellig, …, G. A. Spinas. 2007. Superiority of small islets in human islet transplantation. *Diabetes.* 56:594–603.

7. Smolen, P., J. Rinzel, and A. Sherman. 1993. Why pancreatic islets burst but single β cells do not. The heterogeneity hypothesis. *Biophys. J.* 64:1668–1680.
8. Jo, J., H. Kang, …, D. S. Koh. 2005. How noise and coupling induce bursting action potentials in pancreatic β-cells. *Biophys. J.* 89:1534–1542.
9. Jonkers, F. C., J. C. Jonas, …, J. C. Henquin. 1999. Influence of cell number on the characteristics and synchrony of Ca^{2+} oscillations in clusters of mouse pancreatic islet cells. *J. Physiol.* 520:839–849.
10. Kilimnik, G., A. Kim, …, M. Hara. 2009. Quantification of pancreatic islet distribution in situ in mice. *Am. J. Physiol. Endocrinol. Metab.* 297:E1331–E1338.
11. Miller, K., A. Kim, …, M. Hara. 2009. Islet formation during the neonatal development in mice. *PLoS ONE.* 4:e7739.
12. Kim, A., G. Kilimnik, and M. Hara. 2010. In situ quantification of pancreatic β-cell mass in mice. *J. Vis. Exp.* 10.3791/1970.
13. Hara, M., R. F. Dizon, …, V. P. Bindokas. 2006. Imaging pancreatic β-cells in the intact pancreas. *Am. J. Physiol. Endocrinol. Metab.* 290:E1041–E1047.
14. Hara, M., X. Wang, …, G. I. Bell. 2003. Transgenic mice with green fluorescent protein-labeled pancreatic β-cells. *Am. J. Physiol. Endocrinol. Metab.* 284:E177–E183.
15. Hanahan, D. 1985. Heritable formation of pancreatic β-cell tumors in transgenic mice expressing recombinant insulin/simian virus 40 oncogenes. *Nature.* 315:115–122.
16. Gregory, P. C. 2005. Bayesian Logical Data Analysis for the Physical Sciences: a Comparative Approach with Mathematica Support. Cambridge University Press, Cambridge, UK.
17. Desgraz, R., and P. L. Herrera. 2009. Pancreatic neurogenin 3-expressing cells are unipotent islet precursors. *Development.* 136:3567–3574.
18. Bock, T., B. Pakkenberg, and K. Buschard. 2003. Increased islet volume but unchanged islet number in ob/ob mice. *Diabetes.* 52:1716–1722.
19. Jo, J., M. Y. Choi, and D. S. Koh. 2007. Size distribution of mouse Langerhans islets. *Biophys. J.* 93:2655–2666.
20. Alanentalo, T., A. Asayesh, …, U. Ahlgren. 2007. Tomographic molecular imaging and 3D quantification within adult mouse organs. *Nat. Methods.* 4:31–33.
21. Alanentalo, T., A. Hörnblad, …, D. Holmberg. 2010. Quantification and three-dimensional imaging of the insulitis-induced destruction of β-cells in murine type 1 diabetes. *Diabetes.* 59:1756–1764.
22. Bonnevie-Nielsen, V., L. T. Skovgaard, and A. Lernmark. 1983. Beta-cell function relative to islet volume and hormone content in the isolated perfused mouse pancreas. *Endocrinology.* 112:1049–1056.
23. Kim, S. K., and M. Hebrok. 2001. Intercellular signals regulating pancreas development and function. *Genes Dev.* 15:111–127.
24. Wang, R. N., G. Klöppel, and L. Bouwens. 1995. Duct- to islet-cell differentiation and islet growth in the pancreas of duct-ligated adult rats. *Diabetologia.* 38:1405–1411.
25. Xu, X., J. D'Hoker, …, H. Heimberg. 2008. Beta cells can be generated from endogenous progenitors in injured adult mouse pancreas. *Cell.* 132:197–207.
26. Inada, A., C. Nienaber, …, S. Bonner-Weir. 2008. Carbonic anhydrase II-positive pancreatic cells are progenitors for both endocrine and exocrine pancreas after birth. *Proc. Natl. Acad. Sci. USA.* 105:19915–19919.
27. Li, W. C., J. M. Rukstalis, …, S. Bonner-Weir. 2010. Activation of pancreatic-duct-derived progenitor cells during pancreas regeneration in adult rats. *J. Cell Sci.* 123:2792–2802.
28. Dor, Y., J. Brown, …, D. A. Melton. 2004. Adult pancreatic β-cells are formed by self-duplication rather than stem-cell differentiation. *Nature.* 429:41–46.
29. Lee, C. S., D. D. De León, …, D. A. Stoffers. 2006. Regeneration of pancreatic islets after partial pancreatectomy in mice does not involve the reactivation of neurogenin-3. *Diabetes.* 55:269–272.
30. Teta, M., M. M. Rankin, …, J. A. Kushner. 2007. Growth and regeneration of adult β-cells does not involve specialized progenitors. *Dev. Cell.* 12:817–826.
31. Scaglia, L., C. J. Cahill, …, S. Bonner-Weir. 1997. Apoptosis participates in the remodeling of the endocrine pancreas in the neonatal rat. *Endocrinology.* 138:1736–1741.
32. Teta, M., S. Y. Long, …, J. A. Kushner. 2005. Very slow turnover of β-cells in aged adult mice. *Diabetes.* 54:2557–2567.
33. Chintinne, M., G. Stangé, …, D. Pipeleers. 2010. Contribution of postnatally formed small β cell aggregates to functional β cell mass in adult rat pancreas. *Diabetologia.* 53:2380–2388.
34. Brennand, K., D. Huangfu, and D. Melton. 2007. All β cells contribute equally to islet growth and maintenance. *PLoS Biol.* 5:e163.
35. Deltour, L., P. Leduque, …, J. Jami. 1991. Polyclonal origin of pancreatic islets in aggregation mouse chimeras. *Development.* 112:1115–1121.
36. Ma, D. F., K. Sudo, …, R. Katoh. 2010. Polyclonal origin of hormone-producing cell populations evaluated as a direct in situ demonstration in EGFP/BALB/C chimeric mice. *J. Endocrinol.* 207:17–25.
37. Seymour, P. A., W. R. Bennett, and J. M. Slack. 2004. Fission of pancreatic islets during postnatal growth of the mouse. *J. Anat.* 204:103–116.